

1 **The interaction between urbanization and aerosols during a typical winter haze**  
2 **event in Beijing**

3 Miao Yu<sup>1</sup>, Guiqian Tang<sup>2</sup>, Yang Yang<sup>1</sup>, Qingchun Li<sup>1</sup>, Yonghong Wang<sup>3</sup>, Shiguang  
4 Miao<sup>1</sup>, Yizhou Zhang<sup>1</sup>, Yuesi Wang<sup>2</sup>

5

6

- 7 1. *Institute of Urban Meteorology, China Meteorological Administration, Beijing, China*  
8 2. *State Key Laboratory of Atmospheric Boundary Layer Physics and Atmospheric Chemistry*  
9 *(LAPC), Institute of Atmospheric Physics, Chinese Academy of Sciences, Beijing 100029,*  
10 *China*  
11 3. *Institute for Atmospheric and Earth System Research / Physics, Faculty of Science,*  
12 *University of Helsinki, Finland*

13

14

15

16 *Submitted to Atmospheric Chemistry and Physics*

17

18

19

20

21

22 *Corresponding author:*

23 **Guiqian Tang**

24 *State Key Laboratory of Atmospheric Boundary Layer Physics and Atmospheric Chemistry*  
25 *(LAPC), Institute of Atmospheric Physics, Chinese Academy of Sciences, Beijing 100029, China*

26

## Abstract

Aerosols cause cooling at the surface by reducing shortwave radiation, while urbanization causes warming by altering the surface albedo and releasing anthropogenic heat. The combined effect of the two phenomena needs to be studied in depth. The effects of urbanization and aerosols were investigated during a typical winter haze event. The event, which occurred in Beijing from 15-22 December 2016, was studied via the rapid-refresh multiscale analysis and prediction system-short term (RMAPS-ST) model. The mechanisms of the impacts of aerosols and urbanization were analyzed and quantified. Aerosols reduced urban-related warming during the daytime by 20% (from 30 to 50%) as PM<sub>2.5</sub> concentrations increased from 200 to 400  $\mu\text{g}\cdot\text{m}^{-3}$ . Conversely, aerosols also enhanced urban-related warming at dawn, and the increment was approximately 28%, which contributed to haze formation. Urbanization reduced the aerosol-related cooling effect by approximately 54% during the haze event, and the strength of the impact changed little with increasing aerosol content. The impact of aerosols on urban-related warming was more significant than the impact of urbanization on aerosol-related cooling. Aerosols decreased the urban impact on the mixing layer height by 148% and on the sensible heat flux by 156%. Furthermore, aerosols decreased the latent heat flux; however, this reduction decreased by 48.8% due to urbanization. The impact of urbanization on the transport of pollutants was more important than that of aerosols. The interaction between urbanization and aerosols may enhance the accumulation of pollution and weigh against diffusion.

## 1 Introduction

In recent years, heavy haze pollution events have increasingly occurred in densely populated urban areas, such as the Beijing-Tianjin-Hebei region (BTH region) and Yangtze River Delta region of China (Zhang et al., 2019). These events have caused increasingly severe adverse effects on transportation, the ecological environment and human health (Zhao et al., 2012; Wu et al., 2010; Liu et al., 2012). A statistical analysis of the variation in haze days in Beijing over the past 10 years showed that the number

56 of haze days has significantly increased (Chen and Wang, 2015; Zhai et al., 2019). The  
57 average annual number of haze days was 162 from 1981-1990, 167 from 1991-2000,  
58 and 188 from 2001-2010. The conditions for the formation of heavy haze in the BTH  
59 region are very complex (Miao et al., 2017; Wei et al., 2018; Ren et al., 2019). Although  
60 emissions, meteorological conditions, terrain, and high-density human activities in  
61 urban areas are all important conditions for the evolution of heavy haze (Huang et al.,  
62 2008a; Zhu et al., 2018), meteorological conditions are critical for the evolution of  
63 heavy haze pollution weather under the background of constant emissions (Wang et al.,  
64 2020; Pei et al., 2020).

65

66 The characteristics of the atmospheric boundary layer structure determine the  
67 horizontal fluidity, vertical diffusion ability, stability and capacity (mixed layer  
68 thickness) of the atmosphere, which are the main factors affecting the formation,  
69 intensity and duration of haze and atmospheric pollution (Guo et al., 2016). Coulter R  
70 L. (1979) indicated that the height of the mixing layer would affect the concentration  
71 and diffusion of pollutants, which has been one of the most important physical  
72 parameters in atmospheric numerical models and atmospheric environment evaluations,  
73 and urbanization and aerosols have been indicated to influence the boundary layer  
74 height (Tao et al., 2015).

75

76 Urbanization, as the most drastic means by which human activities transform the  
77 environment, has had an important impact on regional climate and weather processes  
78 (Miao et al., 2011; Yu and Liu, 2015; Yu et al., 2017). Existing research suggests that  
79 there are three main ways by which urbanization influences the climate (Oke, 1982 and  
80 1995). The change in land use from natural surfaces to impervious underlying surfaces  
81 in association with urbanization alters the surface albedo and roughness, which results  
82 in the formation of urban heat islands (UHIs) (Taha, 1997; Folberth et al., 2014). These  
83 alterations lead to a change in the surface energy balance and the form of the thermal  
84 difference between urban and rural areas and further change the boundary layer

85 structure (Grimmond, 2007; Li and Bou-Zeid, 2013). Second, thermal differences  
86 further lead to heat island circulation, which can influence the local circulation of  
87 synoptics and the transport of pollutants (Crutzen, 2004). Anthropogenic aerosols and  
88 heat from the development of transportation and industry are also important parts of  
89 urban impacts on climate (Huang et al. 2008b). However, in contrast to the effects of  
90 urbanization, aerosols cause cooling at the surface by reducing shortwave radiation to  
91 enhance static stability (Grimmond, 2007; Cruten, 2004, Huang et al., 2007).  
92 Furthermore, aerosols may increase longwave radiation in urban areas because they are  
93 likely to absorb and emit more energy than water vapor or greenhouse gases under  
94 certain conditions (Jacobson, 1998; Rudich et al., 2007). There have been few studies  
95 on the mechanism of the interaction between urbanization and aerosols, although many  
96 studies have focused on their respective effects. Accordingly, the interaction between  
97 urbanization and aerosols is important for studying regional climate.

98

99 Researchers are increasingly aware of the importance of the interaction between  
100 urbanization and aerosols. A very important study by Cao et al. (2016) describes the  
101 first attempt to determine the effects of aerosols on urbanization and indicated that  
102 aerosols can increase the nighttime UHI effect using a climate model. Yang et al. (2020)  
103 obtained different results when using observational data to perform similar research in  
104 the BTH region.

105

106 More detailed research needs to be performed by combining observational data and  
107 modeling because the conclusions may vary depending on the scale (Xu et al., 2019).  
108 Other illuminating work with regional models showed that the combined effect of UHIs  
109 and aerosols on precipitation depends on synoptic conditions (Zhong et al., 2015).  
110 However, for winter haze, Zhong et al. (2017) evaluated the impact of urban areas on  
111 air quality and indicated that urbanization can increase ventilation during the daytime  
112 and increase aerosol emissions, and these effects outweigh the UHI effect.

113

114 However, very few studies have quantified the individual effects of urbanization-  
115 induced UHIs and elevated aerosol emissions on the formation and development of  
116 haze in metropolitan areas. A difficulty faced by such studies is that the radiative forcing  
117 of aerosols is not a prognostic variable in most climate models (Cao et al. 2016). Some  
118 regional models, such as WRF-Chem, can overcome this problem by parameterizing  
119 aerosols to aerosol optical depth (AOD) in some specific radiation schemes. Tao et al.  
120 (2015) and Zhong et al. (2018) made some progress in this area, and their results also  
121 indicated that a regional model could be used as an effective way to study the interaction  
122 between urbanization and aerosols. However, a quantitative evaluation of the impacts  
123 or urban areas on aerosols and the simultaneous impacts of aerosols on urban impacts  
124 in metropolitan areas has not been attempted.

125

126 In this study, the rapid-refresh multiscale analysis and prediction system-short term  
127 (RMAPS-ST) was used to investigate the mechanism of the influence of the above two  
128 factors during a typical winter haze event. The objectives of this study are 1) to quantify  
129 the impacts of urban areas on aerosols and the impacts of aerosols on urbanization and  
130 2) to obtain a better understanding of the interaction between urbanization and aerosols  
131 and its influence mechanism on the boundary layer structure and haze transmission  
132 during a typical winter haze event in the BTH region.

133

## 134 **2 Methods**

### 135 **2.1 Observational data**

136 To investigate the interaction between urbanization and aerosols, observation data on  
137 basic meteorological elements, air quality, radiation and surface heat flux and the  
138 mixing layer height (MLH) are very important to reveal the impact of urbanization and  
139 aerosols during haze events.

140

141 The basic meteorological elements were obtained from 309 national basic weather  
142 stations in the BTH region and were provided by the China Meteorological

143 Administration (<http://data.cma.cn/>). The locations of the national basic weather  
144 stations are shown in Fig 1 (red dots). The mass concentrations of fine particulate matter  
145 (PM<sub>2.5</sub>) were recorded by 251 environmental monitor stations managed by the Ministry  
146 of Ecology and Environment of the People's Republic of China  
147 (<http://hbk.cei.cn/aspx/default.aspx>) (Fig 1, black dots). We also used radiation and  
148 surface heat flux data to analyze the urban surface energy budget obtained from the  
149 Beijing meteorological tower (39.97°N, 116.37°E). The tower is 325 m high and is  
150 operated by the Institute of Atmospheric Physics (IAP), Chinese Academy of Sciences  
151 (CAS). The heat flux data were measured by a fast response eddy covariance sensor  
152 system that was sampled at 10 Hz using CR500 (Campbell Scientific Inc., USA). The  
153 radiation data were provided by Kipp & Zonen (Netherlands) four-component  
154 unventilated CNR1 radiometers. Radiation and surface flux data from 140 m of the  
155 tower were used in this study. In addition, the MLH is an important factor affecting  
156 pollutant diffusion and is also affected by both urbanization and aerosols. Because the  
157 MLH is not a routine observation, we obtained the data from only one site. The MLH  
158 and backscattering coefficient were measured by enhanced single-lens ceilometers  
159 (Vaisala, CL51, Finland) deployed by the IAP (Tang et al., 2016). Backscattering  
160 coefficient profiles were calculated by referencing the attenuation strobe laser LiDAR  
161 technique (910 nm), which is cited in Tang et al. (2015).

162

## 163 **2.2 Model description and experimental design**

164 To investigate the respective effects of urbanization and aerosols and further determine  
165 the interaction between urbanization and aerosols, a high-resolution regional model  
166 with satisfactory performance is necessary for sensitivity tests. The model used in this  
167 study is the latest available version of RMAPS-ST, which was developed by the  
168 Institute of Urban Meteorology, China Meteorological Administration. RMAPS-ST is  
169 based on the Weather Research and Forecasting (WRF v3.8.1) model (Skamarock et  
170 al., 2008) and its data assimilation system (WRFDA v3.8). The simulation domain was  
171 centered at 37.0 °N, 105.0 °E and implemented with two nested grids with resolutions of

172 9 and 3 km for two domains (D1 and D2, respectively) (Fig 1a). The model performance  
173 was verified, and RMAPS-ST was run operationally (Fan et al., 2018). The assimilation  
174 began every three hours, and the assimilated data included automatic meteorological  
175 station data, sounding data and radar data when available. The model settings are shown  
176 in Table 1. The simulation started at 0000 LST and ran from the 15<sup>th</sup> to 23<sup>rd</sup> of  
177 December 2016 with hourly outputs.

178

179 The urban impact was represented by a high-resolution (30 m) land use map interpreted  
180 from Landsat Thematic Mapper satellite data from 2015 in Beijing. The urban canopy  
181 parameters were optimized according to Miao and Chen (2014). The impact of aerosols  
182 was represented by adding the hourly distribution of AOD in the Rapid Radiation  
183 Transfer Model for General Circulation Models (RRTMG) radiation scheme. The AOD  
184 was extracted from the output of RMAPS-Chem (Zhao et al., 2019; Zhang et al., 2018)  
185 for the BTH region, which is shown in Fig 1b. Anthropogenic emission data were  
186 obtained according to the Multiresolution Emission Inventory for China (2012)  
187 (<http://www.meicmodel.org/>) with a resolution of  $0.1^{\circ} \times 0.1^{\circ}$ . The particle size  
188 distribution and typology of aerosols used in this study is according to Ruiz et al. (2014).  
189 The simulated distribution of AOD in Beijing was verified to be satisfactory after  
190 comparison with the observed vertical profile of the backscattering coefficient (Fig 2a  
191 and b). The correlation between the AOD and the column backscatter coefficient is 0.76  
192 (Fig 2c). Four tests were designed to investigate the impacts of aerosols and  
193 urbanization on typical haze events. Test 1: Both urban and aerosol impacts were  
194 considered in the simulation. We updated the grid AOD distribution hourly as the input  
195 field for the RRTMG radiation scheme in Domain 2. Test 2: Only aerosol impact was  
196 considered in the simulation, and we replaced the urban grids with cropland to shield  
197 the impact of urbanization. Test 3: Only urban impact was considered, and the direct  
198 radiative forcing of aerosols was not considered in the simulation. Test 4: Both urban  
199 and aerosol impacts were not considered in the simulation.

200

201 The model evaluation results for the four tests are shown in Table 2. As the service  
202 operational system, the RMAPS-ST model assessment report indicated that the model  
203 performance was satisfactory (Fan et al. 2018). We evaluated not only the conventional  
204 meteorological variables (including temperature, humidity and wind speed) but also  
205 unconventional but important variables for this study (including radiation and surface  
206 heat flux). A total of 309 meteorological station data points were used to evaluate the  
207 conventional variables. The unconventional variables were evaluated according to the  
208 observational data from 140 m of the Beijing meteorological tower. Test 1 was found  
209 to be the best simulation and considered both the urban and aerosol impacts. The  
210 deficiency of observation sites, interpolation methods and the height differences  
211 between the observations and simulations resulted in higher root mean square error  
212 (RMSE) values for radiation and heat flux than for the other variables.

213

### 214 **3 Results**

#### 215 **3.1 Observation and weather condition analysis**

216 A typical continuous severe heavy haze event occurred from the 15<sup>th</sup> to 22<sup>nd</sup> of  
217 December 2016 in the BTH region. Three stages dominated by three different synoptic  
218 patterns controlled the formation of this haze. In the first stage, northwest airflow in  
219 front of a ridge of high pressure was observed in the BTH region at a height of 700 to  
220 500 hPa and in eastern China at a height of 850 hPa on the 15<sup>th</sup> to 16<sup>th</sup> of December,  
221 which induced a sharp warming pattern (Fig 3a and b). At the surface, Beijing was  
222 located under the front of the high-pressure system to under the southwest airflow in  
223 front of the low-pressure system (Fig 4), which favored pollutant transport from Hebei  
224 Province to Beijing. From the 17<sup>th</sup> to the night of the 18<sup>th</sup>, the control system turned to  
225 latitude circulation at 700 to 500 hPa over the BTH region (there was a trough line south  
226 of 40°N at 2000 LST on the 17<sup>th</sup> and 18<sup>th</sup>) (Fig 3c). There was a northwest wind located  
227 north of 40°N and a southwest wind located south of 40°N at 850 hPa (Fig 3d). The  
228 near surface was controlled by the northeast airflow located in the inverted low-pressure  
229 trough. The weak convergence of the high trough cooperates with the low pressure at



230 the surface, leading to continuous pollution accumulation near the surface. Under this  
231 weather situation, the near-surface temperature began to continuously increase from the  
232 16<sup>th</sup> to 18<sup>th</sup>, and the specific humidity also correspondingly increased (Fig 5a). The near-  
233 surface wind speed and pressure decreased during this period (Fig 5b). The  
234 concentration of PM<sub>2.5</sub> gradually increased from the 16<sup>th</sup>, and the average concentration  
235 of PM<sub>2.5</sub> reached 200  $\mu\text{g}\cdot\text{m}^{-3}$  on the 18<sup>th</sup>. The density of ozone obviously decreased  
236 from the 16<sup>th</sup> (Fig 5c).

237

238 The MLH significantly declined beginning on the 16<sup>th</sup>, and the diurnal cycle almost  
239 disappeared during this period, which was accompanied by a reduction in visibility with  
240 a diurnal variation (Fig 5d). The downward shortwave radiation and the net radiation  
241 gradually decreased from the 16<sup>th</sup> to the 18<sup>th</sup>, which directly influenced the trend of the  
242 variation in ozone (the maximum density of ozone was less than 110  $\text{mg}\cdot\text{m}^{-3}$ ), while  
243 there was little change detected in longwave radiation (Fig 5e). The observed sensible  
244 heat flux also decreased from the 16<sup>th</sup> to the 19<sup>th</sup>, although the temperature increased,  
245 which means that the heat exchange became weaker in the vertical direction, while the  
246 latent heat flux changed little (Fig 5f). Southwest airflow was again captured by a wind  
247 profiler on the night of the 18<sup>th</sup>, and the transport layer occurred from 300 to 1500 m,  
248 which differs from the previous surface transport pattern (Fig 4).

249

250 In the second stage, an important change occurred on the morning of the 19<sup>th</sup> of  
251 December, when the control system turned to the northwest airflow on the front of the  
252 trough over the BTH region at 500 to 850 hPa (Fig 3e and f). After 2000 LST on the  
253 19<sup>th</sup>, obvious warming occurred again at 850 hPa in eastern China (Fig 3h). However,  
254 the near-surface maximum temperature and diurnal range in Beijing significantly  
255 decreased but with high specific humidity during the 20<sup>th</sup> to 21<sup>st</sup> (Fig 5a). According to  
256 the surface weather map, the control system turned to the southwest at 1400 LST on the  
257 19<sup>th</sup>, and a large-scale southeast wind appeared in eastern Beijing after 2000 LST, which  
258 induced wide advection fog formation overnight (Fig 3g). Due to the influence of the

259 southwest airflow on the trough at 500 hPa, the inverted trough moved east, and Beijing  
260 was located in the southeast wind zone. The near-surface pressure increased slightly,  
261 and the wind speed remained low at approximately  $1 \text{ m}\cdot\text{s}^{-1}$  (Fig 5b). The synoptic  
262 system caused the  $\text{PM}_{2.5}$  concentration to peak (approximately  $400 \mu\text{g}\cdot\text{m}^{-3}$  on average  
263 and above  $500 \mu\text{g}\cdot\text{m}^{-3}$  observed at some stations) and was maintained from the 20<sup>th</sup> to  
264 the 21<sup>st</sup> in the BTH region. The visibility was less than 400 m, and the diurnal cycle  
265 disappeared (Fig 5d). The decrease in the downward shortwave and net radiation during  
266 this period was more pronounced than that in the previous three days (Fig 5e). The  
267 sensible heat flux also decreased, and the diurnal cycle almost disappeared from the  
268 19<sup>th</sup> to the 20<sup>th</sup> (Fig 5e). It was not until the strong cold air moved southward in the  
269 early morning of the 22<sup>nd</sup> when the whole atmosphere converted to the northwest stream.  
270 The air pollutants were completely removed in the third stage.

271

272

### 273 **3.2 Interaction between the impacts of urbanization and aerosols on haze events**

274 Four impacts were analyzed as follows. Urban impact under the aero scenario (UI\_aero)  
275 was represented by the results of Test 1 minus those of Test 2; urban impact under the  
276 no-aero scenario (UI\_noaero) was represented by the results of Test 3 minus those of  
277 Test 4; the impact of the urbanization scenario was represented by the results of Test 1  
278 minus those of Test 3 (AI\_urban); the impact without urbanization was represented by  
279 the results of Test 2 minus those of Test 4 (AI\_nourban). The interaction between  
280 urbanization and aerosols on local meteorological and regional transportation was  
281 discussed.

282

#### 283 **3.2.1 The impact on the local area**

284 The quantitative results of the interaction between urbanization and aerosols are shown  
285 in Table 3. Temperature is one of the most sensitive variables affected by urbanization  
286 and aerosols and is also the most concerning variable. The impact of urbanization on  
287 the near-surface temperature displays diurnal variation in the Beijing area. The warming

288 effect of urbanization was dominant at night. The urban impact on temperature was  
289 partly offset under aerosol conditions when comparing the results of UI\_aero and  
290 UI\_noaero, especially during the daytime (Fig 6a, red lines). The urban impact always  
291 showed a positive contribution to the temperature throughout the day under the no-  
292 aerosol scenario, while the urban impact became slightly negative during the daytime  
293 under the aerosol scenario. The maximum difference between UI\_aero and UI\_noaero  
294 occurred on the 20<sup>th</sup> and 21<sup>st</sup>, when the AOD value reached its maximum, and the  
295 difference almost disappeared on the 15<sup>th</sup> and 22<sup>nd</sup>, with a small AOD (Fig 2b). The  
296 results indicate that the impact of urbanization on temperature is reduced by aerosols,  
297 which is consistent with the findings of Yang et al. (2020). The average urban impact  
298 on temperature in Beijing during the 16<sup>th</sup> to 19<sup>th</sup> with a PM<sub>2.5</sub> concentration of  
299 approximately 200 mg·m<sup>-3</sup> was a reduction of 0.42°C according to UI\_aero and a  
300 reduction of 0.60°C according to UI\_noaero. This result means that aerosols reduce the  
301 urban impact on temperature by 30%. When the concentration of PM<sub>2.5</sub> reached 500  
302 mg·m<sup>-3</sup> from the 20<sup>th</sup> to the 21<sup>st</sup>, the aerosols reduced urbanization-related warming by  
303 54%.

304

305 The impact of aerosols on temperature is negative and without a diurnal cycle under the  
306 urbanization scenario for the whole day (Fig 6a, blue lines). However, the impact of  
307 aerosols captured by AI\_nourban is significant and displays a diurnal cycle. Another  
308 important observation is that the impact of aerosols on temperature under the no-urban  
309 scenario is not always negative. There is a slight warming period at dawn in the  
310 AI\_nourban scenario, which may be because the longwave radiation is increased  
311 (Jacobson, 1998; Rudich et al., 2007). The average impact of aerosols on temperature  
312 in Beijing was -0.16°C with urbanization and -0.34°C without urbanization from the  
313 16<sup>th</sup> to the 19<sup>th</sup>. The impact of aerosols was -0.19°C with urbanization and -0.43°C  
314 without urbanization from the 20<sup>th</sup> to the 21<sup>st</sup>. Urbanization decreased the impact of  
315 aerosols by 53% under moderate pollution and by up to 56% under heavy pollution.  
316 Two different impacts of aerosols on urban-related warming were observed. There was

317 a reducing effect in the daytime with a strength of approximately 30 to 50% of the  
318 concentration, and an increasing effect occurred at dawn with a strength of  
319 approximately 28%. Urbanization reduced the aerosol-related cooling effect by  
320 approximately 54%.

321

322 The observed specific humidity continued to increase as the aerosol concentration  
323 increased (Fig 5b) and was closely related to the UHI effect and aerosol composition  
324 (Zhang et al. 2010; Sun et al., 2013; Wang et al., 2020). The specific humidity also  
325 increased with urbanization throughout the day (Fig 6b, red lines). Similar to  
326 temperature, urbanization had a more pronounced impact on specific humidity at night.  
327 The average urban impact on specific humidity was  $3.66 \times 10^{-2} \text{ g} \cdot \text{kg}^{-1}$  according to  
328 UI\_aero and  $4.78 \times 10^{-2} \text{ g} \cdot \text{kg}^{-1}$  according to UI\_noaero from the 16<sup>th</sup> to 19<sup>th</sup> and  $3.08 \times 10^{-2}$   
329  $^2$  and  $4.48 \times 10^{-2} \text{ g} \cdot \text{kg}^{-1}$  from the 20<sup>th</sup> to 21<sup>st</sup>. Aerosols not only reduced the urban impact  
330 on the average daily specific humidity by 23.43% but also reduced the diurnal range of  
331 specific humidity.

332

333 In contrast to urbanization, aerosols were found to reduce the specific humidity (Fig 6b,  
334 blue lines). The impact of aerosols under the urbanization scenario was small and did  
335 not exhibit a diurnal pattern. However, the impact of aerosols under the no-urban  
336 scenario was more distinct and exhibited a diurnal cycle. The average impact of aerosols  
337 on specific humidity was  $-0.88 \text{ g} \cdot \text{kg}^{-1}$  according to AI\_urban and  $-1.36 \text{ g} \cdot \text{kg}^{-1}$  according  
338 to AI\_nourban throughout the study period. Urbanization reduced the impact of  
339 aerosols on specific humidity by 35.3%. The impacts of urbanization and aerosols on  
340 humidity were slightly greater than those of aerosols on urban impacts.

341

342 There was no effect of urbanization on downward shortwave radiation according to  
343 both UI\_aero and UI\_noaero (Fig 6c, red lines), although the value was not absolutely  
344 related to aerosols because of model uncertainty. Aerosols reduce the downward  
345 shortwave radiation during the daytime, and the differences between AI\_urban and

346 AI\_nourban are very small.

347

348 The average decrease in shortwave radiation caused by aerosols was approximately 7%  
349 of the total downward shortwave radiation during the 16<sup>th</sup> to the 20<sup>th</sup> and up to 17%  
350 when the PM<sub>2.5</sub> was greater than 400  $\mu\text{g}\cdot\text{m}^{-3}$ . The urban impact increased the longwave  
351 radiation at night according to UI\_aero, while the impact of urbanization was always  
352 positive for longwave radiation during the study period according to UI\_noaero (Fig  
353 6d, red lines). Because it is closely related to temperature, the urban impact on  
354 longwave radiation was also reduced by aerosols, with reductions of 83% from the 16<sup>th</sup>  
355 to the 19<sup>th</sup> and 97% from the 20<sup>th</sup> to the 21<sup>st</sup>. The impact of aerosols on longwave  
356 radiation was less than that of shortwave radiation, and there was a slight decrease  
357 captured by AI\_urban with an increase from noon on the 20<sup>th</sup> to nighttime on the 21<sup>st</sup>.  
358 The impact of aerosols decreased the longwave radiation captured by AI\_nourban  
359 during the 16<sup>th</sup> to the 20<sup>th</sup> and increased it on the night of 21<sup>st</sup> (Fig 6d, blue lines).  
360 Urbanization reduced the impact of aerosols on longwave radiation by 67%, while  
361 aerosols reduced the urban impact on longwave radiation by 89%. The impacts of  
362 urbanization and aerosols on longwave radiation are unimportant because they are both  
363 smaller than  $2\text{ W}\cdot\text{m}^{-2}$ .

364

365 The change in radiation further alters the MLH. Previous studies suggested that the  
366 MLH is important for the diffusion of pollutants and haze formation (Sun et al. 2013;  
367 Quan et al. 2014). Previous studies on urbanization indicated that urban-induced  
368 warming will increase the MLH during the daytime (Wang et al., 2007; Miao et al.  
369 2012), and the results of UI\_noaero showed the same pattern. However, when we  
370 introduced aerosols into the simulation, urbanization was found to decrease the MLH  
371 during the daytime according to UI\_aero. The impact of aerosols decreased the average  
372 urbanization by 148% during the haze event (Fig 6e, red lines). Aerosols significantly  
373 decreased the MLH during the daytime according to both AI\_urban and AI\_nourban  
374 (Fig 6e, blue lines). Urbanization decreased the impact of aerosols on the MLH by 58%

375 during the haze event.

376

377 Urban land use change directly alters the surface heat flux. Urbanization increased the  
378 sensible heat flux according to UI\_noaero but decreased the sensible heat flux  
379 according to UI\_aero (Fig 6f, red lines). The impact of aerosols in reducing the urban  
380 impact on sensible heat flux was 156% during the haze event. Aerosols reduced the  
381 sensible heat flux according to both AI\_urban and AI\_nourban (Fig 6f, blue lines). The  
382 maximum impact of aerosols occurred on the 21<sup>st</sup>, with the maximum AOD. The impact  
383 of urbanization reduced the impact of aerosols on sensible heat flux by 59%.

384

385 There was little effect of urbanization on latent heat flux because the observed latent  
386 heat flux in urban areas was small (Fig 6g, red lines, and Fig 5e). Aerosols decreased  
387 the latent heat flux, and the impact increased with increasing AOD (Fig 6g, blue lines).  
388 The impact of urbanization reduced the impact of aerosols on the latent heat flux by  
389 48%.

390

391 The above results indicate that the offsetting effect of aerosols on urbanization is more  
392 important than the impact of urbanization on aerosols on local weather.

393

### 394 **3.2.2 Effects on regional circulation**

395 There are few valuable findings from the diurnal average wind speed analysis because  
396 the average wind speed was low during the haze event. Wind speed is likely to become  
397 more meaningful during the spatial analysis of wind vectors. There are two main  
398 transmission processes of pollution from Hebei Province to Beijing during this haze  
399 process according to the weather map and wind profile analysis (Fig 4). Accordingly,  
400 the diurnal pattern of PM<sub>2.5</sub> in Beijing (Fig 5c) also displays two increasing processes  
401 on the 16<sup>th</sup> and 19<sup>th</sup> (from 1800 to 2400 LST). The observed near-surface wind vector  
402 displays these two pollutant transport processes (Fig 7). In the first processes, obvious  
403 aerosol transport began on the night of the 15<sup>th</sup> and continued to the night of the 16<sup>th</sup>

404 (Fig 6). The southwest wind dominated most of the southern part of Hebei Province.  
405 The transmission flux was strong during the daytime on the 16<sup>th</sup>, leading to the  
406 concentration of PM<sub>2.5</sub> continuing to increase in Beijing and in its transmission path.  
407 The wind speed remained low from the 17<sup>th</sup> to the 18<sup>th</sup> in most of the plain area, and the  
408 concentration of PM<sub>2.5</sub> continued to increase in the southwest and northeast of Hebei  
409 Province. The second processes began at 1400 LST on the 19<sup>th</sup>, and the south wind  
410 dominated the south of Beijing and turned to the southwest in Beijing at 1400 to 1800  
411 LST. The dominant wind direction turned to the southwest at 2200 LST in the southern  
412 part of Hebei Province with a rapid increase in the concentration of PM<sub>2.5</sub>.

413

414 Most industrial aerosols in Beijing are transported from the southwest and northeast of  
415 Hebei Province due to the control of pollutant discharge in the Beijing area during haze  
416 events. Therefore, the impact of urban areas and aerosols on transport, namely, wind  
417 fields, is very important for air quality in Beijing. The modeling results show that  
418 urbanization not only increased the temperature in urban areas (Fig 8a and b) but also  
419 increased the average south-wind transport flux in the two main transmission processes  
420 of pollution in the southwest area of Beijing (Fig 8a and b). The transmission flux  
421 captured by UI\_noaero was stronger than that captured by UI\_aero. The local cyclonic  
422 circulation induced by urbanization further induced upward movement, which was  
423 beneficial to diffusion conditions. Although aerosols decrease the transmission flux  
424 induced by urbanization, the strength of local cyclonic circulation is also reduced by  
425 aerosols. Furthermore, the aerosols reduced the temperature in most of the plain area in  
426 Hebei Province (Fig 8c and d). Urbanization decreased the impact of aerosols on  
427 temperature. There was no local or systemic effect on the wind field captured by either  
428 AI\_urban or AI\_nourban.

429

430 Taylor diagrams were used to analyze the relative contributions of urbanization and  
431 aerosols over time (Fig 9). The daily mean differences in these four types of impact  
432 (UI\_aero, UI\_noaero, AI\_urban, and AI\_nourban) over the eight days in the Beijing

433 area are shown by Taylor diagrams. UI\_noaero shows that temperature continued to  
434 increase from Day 1 to Day 5 and reached a maximum on Day 7. The variation in  
435 temperature according to UI\_aero was small. This result means that the effect of  
436 urbanization on temperature is decreased by aerosols. Temperature increased from Day  
437 1 to Day 7 according to AI\_urban, while AI\_nourban showed an increase from Day 3  
438 to Day 7. The reduction in the urban impact on temperature by aerosols was more  
439 important than the reduction in aerosol impact on temperature by urbanization (Fig 9a).  
440 The effect of aerosols on the urban impacts on temperature was more important than  
441 the urban impacts on the effects of aerosols on temperature (Fig 9a).

442

443 Specific humidity continued to increase from Day 1 to Day 5 according to UI\_noaero,  
444 while the variation in specific humidity was small according to UI\_aero (Fig 9b).  
445 Similar to what was observed for temperature, reducing the urban impact on specific  
446 humidity by aerosols is more important than reducing the impacts to aerosols by urban  
447 areas. The ventilation coefficient (VC) in UI\_aero showed little change over these eight  
448 days, and this coefficient showed increases on Days 2, 3, 5, and 6 and decreases on  
449 Days 4, 7, and 8 according to UI\_noaero. The reduction in the urban impact on the VC  
450 by aerosols was more important than the reduction in the impact of aerosols by  
451 urbanization. The analysis of shortwave radiation also provided the same conclusion  
452 that the reduction in the urban impact on the daily mean by aerosols was more important  
453 than the reduction in the impact of aerosols by urbanization (Fig 9d).

454

### 455 **3.2.3 Impacts on the vertical distribution**

456 In the period from 0000 LST to 0800 LST on the 16<sup>th</sup> to 20<sup>th</sup>, there was an interesting  
457 phenomenon that temperature was slightly larger in UI\_aero than in UI\_noaero, and the  
458 urban impact reached a maximum at the same time. Such an outcome is easy to overlook  
459 if the analysis focuses on only the daily average. Therefore, a detailed vertical  
460 temperature and wind field analysis of the four addressed scenarios (UI\_aero,  
461 UI\_noaero, AI\_urban, and AI\_nourban) was used to determine the mechanism behind



462 this finding (Fig 10).

463

464 The impact on warming by urbanization reached 350 m in UI\_aero and 450 m in  
465 UI\_noaero (Fig 10a and b). Aerosols not only increased the warming impact induced  
466 by urbanization but also reduced the warming height. Aerosols increase the near-surface  
467 warming effect induced by urbanization because of the absorption of longwave  
468 radiation. Although absorption by aerosols was always observed during the study period,  
469 the impact increased with the increase in longwave radiation induced by urbanization.  
470 Therefore, the warming effect of aerosols may dominate at night in the near-surface  
471 layer. This effect further induces urban-related warming to increase and compress this  
472 effect to a lower height with a lower MLH in UI\_aero than in UI\_noaero (Fig 10a). The  
473 aerosols reduced the temperature below 450 m in the urban area of Beijing (Fig 10c and  
474 d), and the cooling effect was reduced by urbanization below 450 m. Urbanization also  
475 reduced the near-surface west wind induced by aerosols in urban areas because of the  
476 drag caused by buildings.

477

#### 478 **4 Conclusion**

479 A typical persistent haze process occurred on the 15<sup>th</sup> to 22<sup>nd</sup> of December 2016 in the  
480 BTH region. The average concentration of PM<sub>2.5</sub> was approximately 200  $\mu\text{g}\cdot\text{m}^{-3}$ , and  
481 the maximum was 695  $\mu\text{g}\cdot\text{m}^{-3}$ . The interaction between aerosols and urbanization on  
482 haze events was investigated in this study. Four tests were designed using RMAPS-ST  
483 to study the mechanism of the impacts of aerosols and urbanization.

484

485 Two different impacts of aerosols on urban-related warming were found. A reducing  
486 effect occurred during the daytime, and the strength was approximately 30 to 50% of  
487 the concentration. An increasing effect occurred at dawn, and the strength was  
488 approximately 28%, which is important for haze formation. The combined effect was a  
489 reducing effect on the daily mean of urban-related warming. Urbanization reduced the  
490 aerosol-related cooling effect by approximately 54% during the haze event, and the

491 strength of the impact changed little with increasing aerosol content. The impact of  
492 urbanization on the effect of aerosols on humidity is slightly larger than the impact of  
493 aerosols on urban impact. Aerosols reduce the average downward shortwave radiation  
494 from 7% to 17% with concentrations of PM<sub>2.5</sub> of 200 to 400  $\mu\text{g}\cdot\text{m}^{-3}$ . There is no urban  
495 impact on downward shortwave radiation or an impact of aerosols on shortwave  
496 radiation. The impacts of urban areas and aerosols on longwave radiation are both  
497 smaller than  $2\text{ W}\cdot\text{m}^{-2}$ . The most significant impact of aerosols is observed on the MLH  
498 and sensible heat flux. The decrease in urban impact caused by aerosols reaches 148%  
499 for MLH and 156% for sensible heat flux. These values are much larger than those for  
500 urbanization, which reduces the impact of aerosols on the MLH and sensible heat flux.  
501 There is little urban impact on latent heat flux. However, aerosols decreased the latent  
502 heat flux, and the impact was reduced by 48.8% by urbanization. In general, the impact  
503 of aerosols on urban impact is more important than the impact of urbanization on  
504 aerosol impacts in terms of regional averages.

505

506 Urbanization increased the wind speed southwest of the Beijing area and the local  
507 cyclonic circulation in the urban area of Beijing during the two main transmission  
508 processes. Although aerosols reduced the urban-related southwest transmission, they  
509 worsened the diffusion conditions in urban areas. The impact of urbanization on wind  
510 fields, namely, the transport of pollutants, is more important than that of aerosols.  
511 However, the interaction between urbanization and aerosols may enhance the  
512 accumulation of pollution and weigh against diffusion.

513

514 The impact of aerosols on urban-related warming is more significant than the impact of  
515 urbanization on aerosol-related cooling according to spatial statistical analysis. Similar  
516 results were found for absolute humidity, VC and shortwave radiation. Aerosol-related  
517 warming is dominant at dawn in the near-surface layer. Aerosols increase urban-related  
518 warming and reduce the impact height of urban-related warming. This further enhances  
519 stability and reduces the MLH.

520 **5 Discussion**

521 In this study, it was easier to distinguish the impacts of aerosols and urbanization by  
522 using RMAPS-ST with AOD hourly inputs than with RMAPS-Chem. One reason for  
523 this difference is that the model performance of RMAPS-ST is much better than that of  
524 RMAPS-Chem in meteorological fields. Although real-time feedback in modeling is  
525 not provided, RMAPS-ST is more efficient and more suitable for short-term operational  
526 forecasting.

527

528 This study not only qualified the impacts of aerosols and urbanization on haze events  
529 but also analyzed the interaction between aerosols and urbanization during haze events.  
530 This research will help to improve air quality under the continuous  
531 urbanization and sustainable development of large cities.

532

533 The government has taken a series of emission reduction measures, including limiting  
534 industrial emissions and vehicle plate number traffic restriction measures, to improve  
535 the air quality in the BTH region. The policies have been effective in reducing aerosols.  
536 At the same time, urbanization continues mainly in the areas around Beijing (such as  
537 the Xiongan New Area). The results of this study show that the combined impact of  
538 urbanization and decreasing aerosols will increase the downward shortwave radiation  
539 and further increase the surface temperature and ozone concentration in the boundary  
540 layer. Previous studies indicated that ozone generally increases with temperature and  
541 decreases with humidity (Camalier et al., 2007; Cardelino et al., 1990). It is well known  
542 that ozone is not only a pollutant but also a greenhouse gas. Therefore, ozone will form  
543 a positive feedback mechanism to induce warming and ozone pollution in the boundary  
544 layer. This feedback will pose a new challenge regarding how to reduce ozone pollution  
545 in urban areas. Some studies have suggested that urban greening can effectively reduce  
546 ozone pollution (Nowak et al., 2000; Benjamin and Winer, 1998). More attempts should  
547 be made to add the interaction between urbanization and ozone in regional models.

548

549 **Acknowledgments**

550 This work was supported by the Beijing National Science Foundation of China  
551 (Grant No. 8171002), the National Natural Science Foundation of China  
552 (Grant No.41705090, 41705076 and 41705088), and the National Key R&D Program  
553 of China (2019YFA0607202).

554

555 **Data availability**

556 The data in this study are available from the corresponding author upon request  
557 ([tgq@dq.cern.ac.cn](mailto:tgq@dq.cern.ac.cn)).

558

559 **Author contribution**

560 Miao Yu designed the research and wrote the paper. Guiqian Tang conducted the  
561 measurements and reviewed the paper. Yang Yang conducted modeling tests. Qingchun  
562 Li and Yonghong Wang performed synoptic analysis. Shiguang Miao, Yizhou Zhang  
563 and Yusi Wang reviewed and commented on the paper.

564

565 **Competing interests**

566 The authors declare that they have no conflicts of interest to disclose.

567

568 Table 1 RMAPS-ST model settings.

WRF v3.8.1	D01	D02
Horizontal grid	649×400	550×424
Grid horizontal spacing (km)	9	3
Vertical layers	49	
PBL	YSU (Hong et al., 2006)	
Microphysics	Thompson (Thompson et al., 2008)	
Cumulus	Kain-Fritsch (Kain, 2004)	None
LW radiation	RRTMG	
SW radiation	RRTMG	

LSM	Noah LSM+SLUCM
Urban parameter values	Modified according to Miao and Chen (2014)

569

570

571

572

573

574

Table 2 Model evaluation (RMSE and BIAS) for the four tests.

	Test 1		Test 2		Test 3		Test 4	
	RMSE	BIAS	RMSE	BIAS	RMSE	BIAS	RMSE	BIAS
Temperature	<b>1.27</b>	<b>0.35</b>	1.45	-0.73	2.12	1.04	1.78	-0.45
Specific	<b>0.26</b>	-	0.31	0.019	0.34	-0.05	0.29	0.03
Wind speed	<b>1.62</b>	<b>0.97</b>	2.08	1.68	1.85	1.04	1.96	1.67
Shortwave	<b>40.91</b>	<b>11.85</b>	40.95	11.89	47.35	17.45	46.26	16.45
Longwave	<b>51.39</b>	-	51.32	-	51.24	-	52.76	44.97
Sensible heat	<b>8.09</b>	<b>-1.19</b>	9.13	-3.92	9.34	-3.43	12.3	-6.17
Latent heat	<b>14.09</b>	<b>-5.75</b>	14.52	-5.95	14.85	-5.87	16.76	-6.23

575

576

577

578

579

580

Table 3 Quantitative results of the interaction between urbanization and aerosols

Time	Temperature °C		Specific humidity ×10 <sup>-2</sup> g kg <sup>-1</sup>		Longwave W·m <sup>-2</sup>		MLH m	Sensible heat flux W·m <sup>-2</sup>	Latent heat flux W·m <sup>-2</sup>
	16 <sup>th</sup> -19 <sup>th</sup>	20 <sup>th</sup> -21 <sup>st</sup>	16 <sup>th</sup> -19 <sup>th</sup>	20 <sup>th</sup> -21 <sup>st</sup>	16 <sup>th</sup> -19 <sup>th</sup>	20 <sup>th</sup> -21 <sup>st</sup>	16 <sup>th</sup> -21 <sup>st</sup>	16 <sup>th</sup> -21 <sup>st</sup>	16 <sup>th</sup> -21 <sup>st</sup>
UI_aero	0.42	0.19	3.66	3.08	0.10	-0.02	-1.97	-1.01	0.03
UI_noaero	0.60	0.35	4.78	4.48	0.62	0.51	4.04	1.74	0.49
AI_urban	-0.16	-0.19	-0.88		-0.24		-4.37	-1.64	-0.50
AI_nourban	-0.34	-0.43	1.36		-0.73		-10.38	-4.02	-0.96

581

582

583 **References**

- 584 Benjamin, M. T., Winer, A. M.: Estimating the ozone-forming potential of urban trees and shrubs,  
585 Atmospheric Environment, 32(1), 53-68, 1998.
- 586 Camalier, L., Cox, W. , and Dolwick, P.: The effects of meteorology on ozone in urban areas and  
587 their use in assessing ozone trends, Atmospheric Environment, 41(33), 7127-7137, 2007.
- 588 Cao, C., Lee, X., Liu, S., Schultz, N., Xiao, W., Zhang, M., and Zhao, L.: Urban heat islands in  
589 China enhanced by haze pollution, Nature Communications, 7(1), 1-7, 2016.
- 590 Cardelino, C. A., and Chameides, W. L.: Natural hydrocarbons, urbanization, and urban  
591 ozone, Journal of Geophysical Research, 95(D9), 13971, 1990.
- 592 Chen, H., and H. Wang: Haze Days in North China and the associated atmospheric circulations  
593 based on daily visibility data from 1960 to 2012, J. Geophys. Res. Atmos., 120, 5895–5909,  
594 2015.
- 595 Coulter, R.L.: A Comparison of three methods for measuring mixing-layer height, J Appl  
596 Meteor,18(11):1495-1499, 1979.
- 597 Crutzen, P. J.: New directions: the growing urban heat and pollution ‘island’ effect-impact on  
598 chemistry and climate, Atmos. Environ, 38, 3539–3540, 2004.
- 599 Fan, S.: Assessment report of regional high resolution model (RMAPS-ST), IUM Technical Note  
600 IUM/2018-1, Beijing, China: IUM, 2018.
- 601 Folberth, G. A., Rumbold, S. T., Collins, W. J., and Butler, T. M.: Global radiative forcing and  
602 megacities, Urban Climate., 1, 4–19, 2014.
- 603 Grimm, N. B. et al.: Global change and the ecology of cities, Science, 319 (5864), 756–760, 2008.
- 604 Grimmond, C.S. B., Kuttler, W., Lindqvist, S., and Roth, M.: Urban climatology icuc6, International  
605 Journal of Climatology, 27(14), 1847-1848, 2010.
- 606 Grimmond, S.U. E.: Urbanization and global environmental change: local effects of urban warming,  
607 Geographical Journal, 173(1), 83-88, 2007.
- 608 Guo, J., Miao, Y., Zhang, Y., Liu, H., Li, Z., Zhang, W., ...and Zhai, P.: The climatology of planetary  
609 boundary layer height in China derived from radiosonde and reanalysis data, Atmospheric  
610 Chemistry and Physics, 16(20), 13309-13319, 2016.
- 611 Huang, J., Minnis, P., Yi, Y., Tang, Q., Wang, X., Hu, Y., ... and Winker, D. M.: Summer dust aerosols  
612 detected from CALIPSO over the Tibetan Plateau, Geophysical Research Letters, 34(18),  
613 DOI:10.1029/2007GL029938, 2007.
- 614 Huang, J., Minnis, P., Chen, B., Huang, Z., Liu, Z., Zhao, Q., ... and Ayers, J. K.: Long-range  
615 transport and vertical structure of Asian dust from CALIPSO and surface measurements during  
616 PACDEX, Journal of Geophysical Research, 113, DOI:10.1029/2008JD010620., 2008a.
- 617 Huang J., W. Zhang, J. Zuo, J. Bi, J. Shi, X. Wang, Z. Chang, Z. Huang, S. Yang, B. Zhang, G. Wang,  
618 G. Feng, J. Yuan, L. Zhang, H. Zuo, S. Wang, C. Fu and J. Chou.: An overview of the semi-arid  
619 climate and environment research observatory over the Loess Plateau, Advances in Atmospheric  
620 Sciences, 25(6), 1-16. DOI: 10.1007/s00376-008-0906-7, 2008b.
- 621 Hong, S. Y., Noh, Y., and Dudhia, J.: A new vertical diffusion package with an explicit treatment of  
622 entrainment processes, Monthly Weather Review, 134, 2318–2341, 2006.
- 623 Jacobson, M. Z.: Studying the effects of aerosols on vertical photolysis rate coefficient and  
624 temperature profiles over an urban airshed, Journal of Geophysical Research, 103,10593–10604,

625 1998.

626 Kain, J. S.: The Kain–Fritsch convective parameterization: An update, *Journal of Applied*  
627 *Meteorology*, 43, 170–181, 2004.

628 Li, D. and Bou-Zeid, E.: Synergistic interaction between urban heat islands and heat waves: the  
629 impact in cities is larger than the sum of its parts, *J. Appl. Meteorol. Climatol*, 52, 2051–2064,  
630 2013.

631 Liu, Q., Geng, H., Chen Y.: Vertical distribution of aerosols during different intense dry haze period  
632 around Shanghai, *China Environmental Science (in Chinese)*, 32(2), 207-213, 2012.

633 Miao, S, Dou J., Chen, F., Li, J., and Li A.: Analysis of observations on the urban surface energy  
634 balance in Beijing, *Science China Earth Sciences*, 055(11), 1881-1890, 2012.

635 Miao, S. and Chen, F.: Enhanced modeling of latent heat flux from urban surfaces in the  
636 Noah/single-layer urban canopy coupled model, *Science China Earth Sciences*, 057(10), 2408-  
637 2416, 2014.

638 Miao, S., Chen, F., Li, Q., and Fan, S.: Impacts of urban processes and urbanization on summer  
639 precipitation: A case study of heavy rainfall in Beijing on 1 August 2006, *Journal of Applied*  
640 *Meteorology and Climatology*, 50, 806–825, <https://doi.org/10.1175/2010JAMC2513.1>, 2011

641 Miao, Y., Guo, J., Liu, S., Liu, H., Li, Z., Zhang, W., and Zhai, P.: Classification of summertime  
642 synoptic patterns in Beijing and their associations with boundary layer structure affecting aerosol  
643 pollution., *Atmos. Chem. Phys*, 17(4), 3097-3110, 2017.

644 Nowak, D. J., Civerolo, K. L., Rao, S. T., Sistla, G., Luley, C. J., and Crane, D. E.: A modeling study  
645 of the impact of urban trees on ozone, *Atmospheric Environment*, 34(10), 1601-1613, 2000.

646 Oke, T.R.: The energetic basis of the urban heat island, *Quarterly Journal of the Royal*  
647 *Meteorological Society*, 108, 1–24, 1982.

648 Oke, T.R.: The heat island of the urban boundary layer: Characteristics, causes and effects, *Wind*  
649 *Climate in Cities*, 81-107, 1995.

650 Pei, L., Yan, Z., Chen, D., & Miao, S.: Climate variability or anthropogenic emissions: which caused  
651 Beijing Haze? *Environmental Research Letters*, 15(3), 034004, 2020.

652 Quan, J., Tie, X., Zhang, Q., Liu, Q., Li, X., and Gao, Y., et al.: Characteristics of heavy aerosol  
653 pollution during the 2012–2013 winter in Beijing, China, *Atmospheric Environment*,  
654 88(Complete), 83-89, 2014.

655 Ren, Y., Zhang, H., Wei, W., Wu, B., Cai, X., and Song, Y.: Effects of turbulence structure and  
656 urbanization on the heavy haze pollution episodes, *Atmospheric Chemistry and Physics*, 19,  
657 1041-1057, 2019.

658 Rudich, Y., Donahue, N. M. & Mentel, T. F. Aging of organic aerosol: bridging the gap between  
659 laboratory and field studies, *Ann. Rev. Phys. Chem.*, 58,321–352, 2007.

660 Ruiz-Arias, J. A., Dudhia, J., & Gueymard, C. A.: A simple parameterization of the short-wave  
661 aerosol optical properties for surface direct and diffuse irradiances assessment in a numerical  
662 weather model. *Geoscientific Model Development*, 7(3), 1159-1174, 2014. Skamarock, W. C.,  
663 Klemp, J. B., Dudhia, J., Gill, D. O., Barker, D., Wang, W., and Powers, J. G.: A description of  
664 the advanced research WRF version 3, NCAR/TN-475 + STR, 2008.

665 Sun, Y., Wang, Z., Fu, P., Jiang, Q., Yang, T., Li, J., and Ge, X.: The impact of relative humidity on  
666 aerosol composition and evolution processes during wintertime in Beijing, China, *Atmospheric*  
667 *Environment*, 77, 927-934, 2013.

668 Taha, H.: Urban climates and heat islands: albedo, evapotranspiration, and anthropogenic heat,  
669 Energy and Buildings, 25, 99–103, 1997.

670 Tang, G., Zhu, X., Hu, B., Xin, J., and Wang, Y.: Impact of emission controls on air quality in Beijing  
671 during APEC 2014: lidar ceilometer observations, Atmospheric Chemistry and Physics, 15(21),  
672 12667-12680, 2015.

673 Tang, G. , Zhang, J. , Zhu, X. , Song, T. , and Wang, Y. : Mixing layer height and its implications  
674 for air pollution over Beijing, China, Atmospheric Chemistry and Physics, 16(4), 2459–2475,  
675 2016.

676 Tao, W., Liu, J., Ban-Weiss, G. A., Hanglustaine, D. A., Zhang, L., Zhang, Q.,... and Tao, S.: Effects  
677 of urban land expansion on the regional meteorology and air quality of eastern China,  
678 Atmospheric Chemistry and Physics, 15(15), 8597–8614, [https://doi.org/10.5194/acp-15-8597-](https://doi.org/10.5194/acp-15-8597-2015)  
679 2015, 2015.

680 Thompson, G., Field, P. R., Rasmussen, R. M., & Hall, W. D.: Explicit forecasts of winter  
681 precipitation using an improved bulk microphysics scheme. Part II: Implementation of a new  
682 snow parameterization, Monthly Weather Review, 136, 5095–5115, 2008.

683 Wang, K., Wang, J., Wang, P., Sparrow, M., Yang, J., Chen, H.: Influences of urbanization on  
684 surface characteristics as derived from the Moderate-Resolution Imaging Spectroradiometer:  
685 A case study for the Beijing metropolitan area, Journal of Geophysical Research, 112 (D22),  
686 doi:10.1029/2006jd007997, 2007.

687 Wang, Y., Yu, M., Wang, Y., Tang, G., Song, T., Zhou, P., ... and Zhu, X.: Rapid formation of intense  
688 haze episodes via aerosol–boundary layer feedback in Beijing, Atmospheric Chemistry and  
689 Physics, 20(1), 45-53, 2020.

690 Wei, W., Zhang, H., Wu, B., Huang, Y., Cai, X., Song, Y., and Li, J.: Intermittent turbulence  
691 contributes to vertical dispersion of PM<sub>2.5</sub> in the North China Plain: cases from Tianjin,  
692 Atmospheric Chemistry and Physics, 18, 12953–12967, [https://doi.org/10.5194/acp-18-12953-](https://doi.org/10.5194/acp-18-12953-2018)  
693 2018, 2018.

694 Wu, D., Wu, X, Li, F., et al.: Temporal and spatial variation of haze during 1951-2005 in Chinese  
695 mainland, Acta Meteorologica Sinica (in Chinese), 68(5), 680-688, 2010.

696 Xu, X., Chen, F., Barlage, M., Gochis, D., Miao, S., and Shen, S.: Lessons learned from modeling  
697 irrigation from field to regional scales, Journal of Advances in Modeling Earth Systems, 11,  
698 2428–2448, <https://doi.org/10.1029/2018MS001595>, 2019.

699 Yang, Y., Zheng, Z., Yim, S. Y. L., Roth, M., Ren, G., Gao, Z., et al.: PM<sub>2.5</sub> pollution modulates  
700 wintertime urban heat island intensity in the Beijing - Tianjin - Hebei Megalopolis, China,  
701 Geophysical Research Letters, 47, e2019GL084288. <https://doi.org/10.1029/2019GL084288>,  
702 2020.

703 Yu, M., and Y. Liu: The possible impact of urbanization on a heavy rainfall event in Beijing,  
704 Journal of Geophysical Research: Atmospheres , 120, 8132–8143, doi:10.1002/2015JD023336,  
705 2015.

706 Yu, M., Miao, S., and Li, Q.: Synoptic analysis and urban signatures of a heavy rainfall on 7 August  
707 2015 in Beijing, Journal of Geophysical Research: Atmospheres, 122, 65–78,  
708 <https://doi.org/10.1002/2016JD025420>, 2017.

709 Yu, M., Y. M. Liu, Y. F. Dai, et al.: Impact of urbanization on boundary layer structure in Beijing,  
710 Climatic Change, 120(1-2), 123-136, 2013.



711 Zhai, S.X, Jacob, Daniel, Wang, X., Lu, S., Li, K., Zhang, Y.Z., Gui, K., Zhao, T.L., and Liao,  
712 H.: Fine particulate matter (PM<sub>2.5</sub>) trends in China, 2013–2018: contributions from meteorology,  
713 Atmospheric Chemistry and Physics, 19(16), 11031-11041, 2019.

714 Zhang, C., Liu, C., Hu, Q., Cai, Z., Su, W., Xia, C., ... and Liu, J.: Satellite UV-Vis spectroscopy:  
715 implications for air quality trends and their driving forces in China during 2005–2017, Light-  
716 Science & Applications, 8(1), 1-12, 2019. Zhang, N., Gao, Z., Wang, X., and Chen, Y.: Modeling  
717 the impact of urbanization on the local and regional climate in Yangtze River Delta,  
718 China, Theoretical and applied climatology, 102(3-4), 331-342, 2010.

719 Zhang, W., Zhuang, G., Guo, J., Xu, D., Wang, W., and Baumgardner, D.,... and Yang, W.: Sources  
720 of aerosol as determined from elemental composition and size distributions in  
721 Beijing, Atmospheric Research, 95(2-3), 0-209, 2010.

722 Zhang, Z., Zhao, X., Xiong, Y., Ma, X.H.: The Fog/Haze Medium-range Forecast Experiments  
723 Based on Dynamic Statistic Method, Journal of Applied Meteorological Science (in Chinese),  
724 29(1),57-69, 2018.

725 Zhao, P., Xu, X., Meng, W. Dong, ... and Zhang, X.L.: Characteristics of haze days in the region of  
726 Beijing, Tianjin, and Hebei, China Environmental Science (in Chinese), 31(1), 31-36, 2012.

727 Zhao, X., Li, Z., and Xu, J.: Beijing regional environmental meteorology prediction system and its  
728 performance test of PM<sub>2.5</sub> concentration, Journal of Applied Meteorological Science (in  
729 Chinese), 27(2),160-172, 2016.

730 Zhao, X.J., Li, Z.M., Xu, J.: Modification and performance tests of visibility parameterizations for  
731 haze days. Environmental. Science, 40 (4), 1688–1696 (in Chinese), 2019.

732 Zhong, S., Qian, Y., Sarangi, C., Zhao, C., Leung, R., Wang, H.,... and Yang, B.: Urbanization effect  
733 on winter haze in the Yangtze River Delta region of China, Geophysical Research Letters, 45,  
734 6710–6718, <https://doi.org/10.1029/2018GL077239>, 2018.

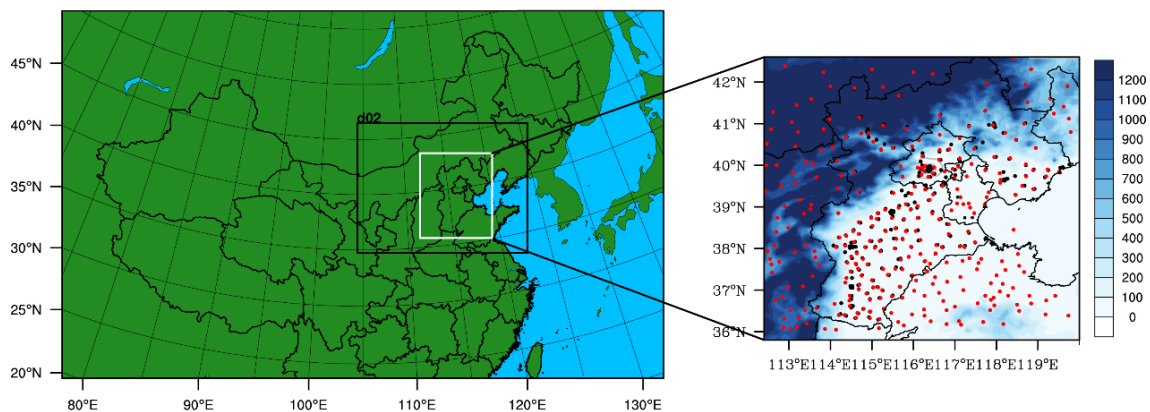
735 Zhong, S., Qian, Y., Zhao, C., Leung, R., and Yang, X. Q.: A case study of urbanization impact on  
736 summer precipitation in the Greater Beijing Metropolitan Area: Urban heat island versus aerosol  
737 effects, Journal of Geophysical Research: Atmospheres, 120, 10,903–10,914.  
738 <https://doi.org/10.1002/2015JD023753>, 2015.

739 Zhong, S., Qian, Y., Zhao, C., Leung, R., Wang, H. L., Yang, B., ... and Liu, D.: Urbanization-  
740 induced urban heat island and aerosol effects on climate extremes in the Yangtze River Delta  
741 region of China. Atmospheric Chemistry and Physics, 17(8), 5439–5457,  
742 <https://doi.org/10.5194/acp-17-5439-2017/>, 2017.

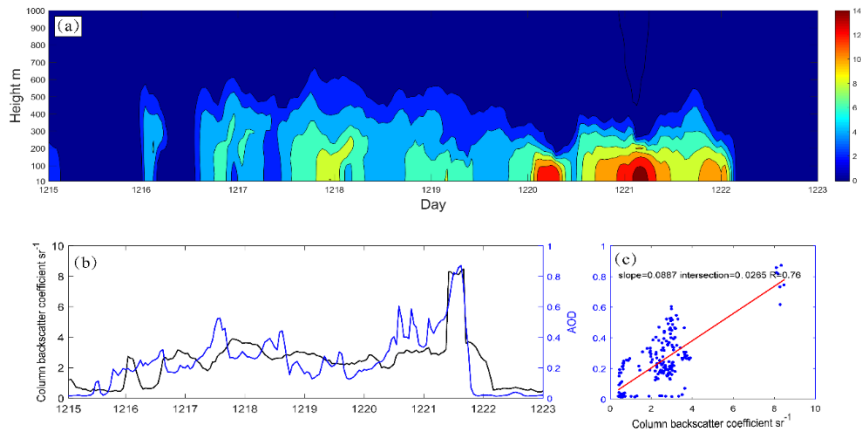
743 Zhu, X., Tang, G., Guo, J., Hu, B., Song, T., Wang, L., Xin, J., Gao, W., Munkel, C., Schäfer, K., Li,  
744 X., and Wang, Y.: Mixing layer height on the North China Plain and meteorological evidence of  
745 serious air pollution in southern Hebei, Atmospheric Chemistry and Physics, 18, 4897–4910,  
746 <https://doi.org/10.5194/acp-18-4897-2018>, 2018.

747  
748  
749  
750  
751  
752  
753

754 **Figure**



755  
756 Figure 1 Domain configuration of RMAPS-ST and the location of the study area, indicated by the  
757 solid white line. The black dots indicate the locations of the 251 environmental monitoring stations,  
758 and the red dots represent the 309 meteorological stations in the BTH region, where the gray loop  
759 lines show the locations of the second to sixth ring roads. The shading is the terrain height (unit: m).  
760  
761  
762  
763  
764

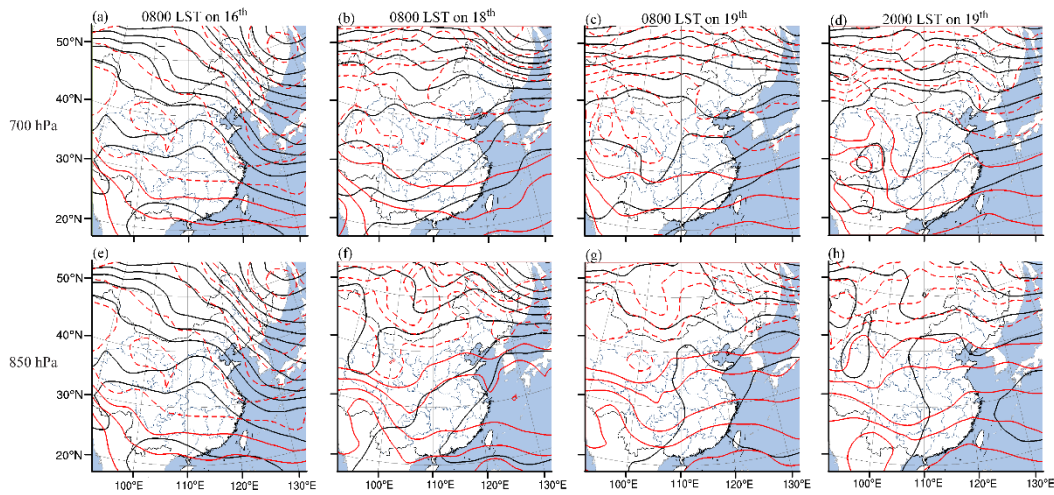


765

766 Figure 2 (a) Hourly backscattering coefficient (shading;  $\text{Mm}\cdot\text{sr}^{-1}$ ) observed by single-lens  
 767 ceilometers ( $39.97^\circ\text{N}$ ,  $116.37^\circ\text{E}$ ) from the 15<sup>th</sup> to 23<sup>rd</sup> of December; (b) hourly column backscatter  
 768 coefficient (black line;  $\text{sr}^{-1}$ ) and AOD used in modeling for Beijing (blue line) and (c) scatter  
 769 diagram of hourly column backscatter coefficient and AOD (blue dots) and their correlations (red  
 770 line).

771

772



773

774 Figure 3 Weather maps. (a) 0800 LST on the 16<sup>th</sup> at 700 hPa; (b) 0800 LST on the 18<sup>th</sup> at 700 hPa;

775 (c) 0800 LST on the 19<sup>th</sup> at 700 hPa; (d) 2000 LST on the 19<sup>th</sup> at 700 hPa; (e) 0800 LST on the

776 16<sup>th</sup> at 850 hPa; (f) 800 LST on the 18<sup>th</sup> at 850 hPa; (g) 0800 LST on the 19<sup>th</sup> at 850 hPa; (h) 2000

777 LST on the 19<sup>th</sup> at 850 hPa.

778

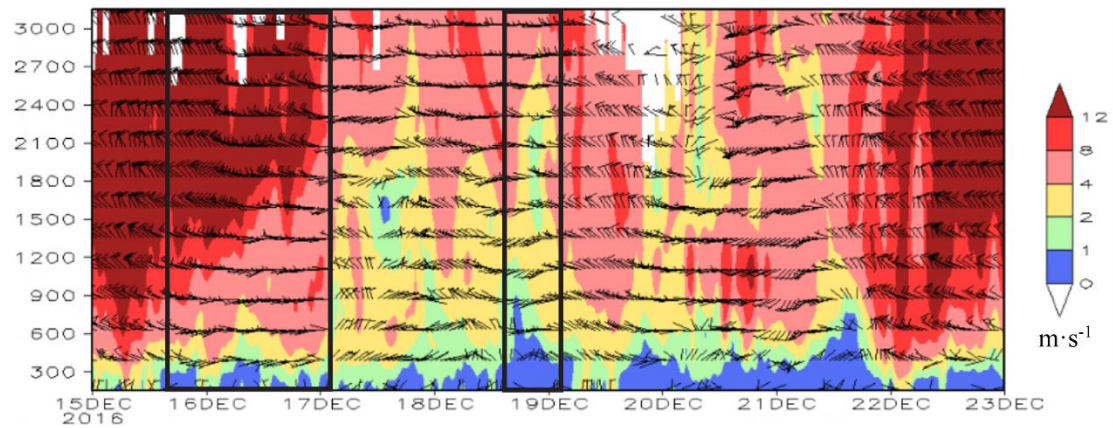
779

780

781

782

783

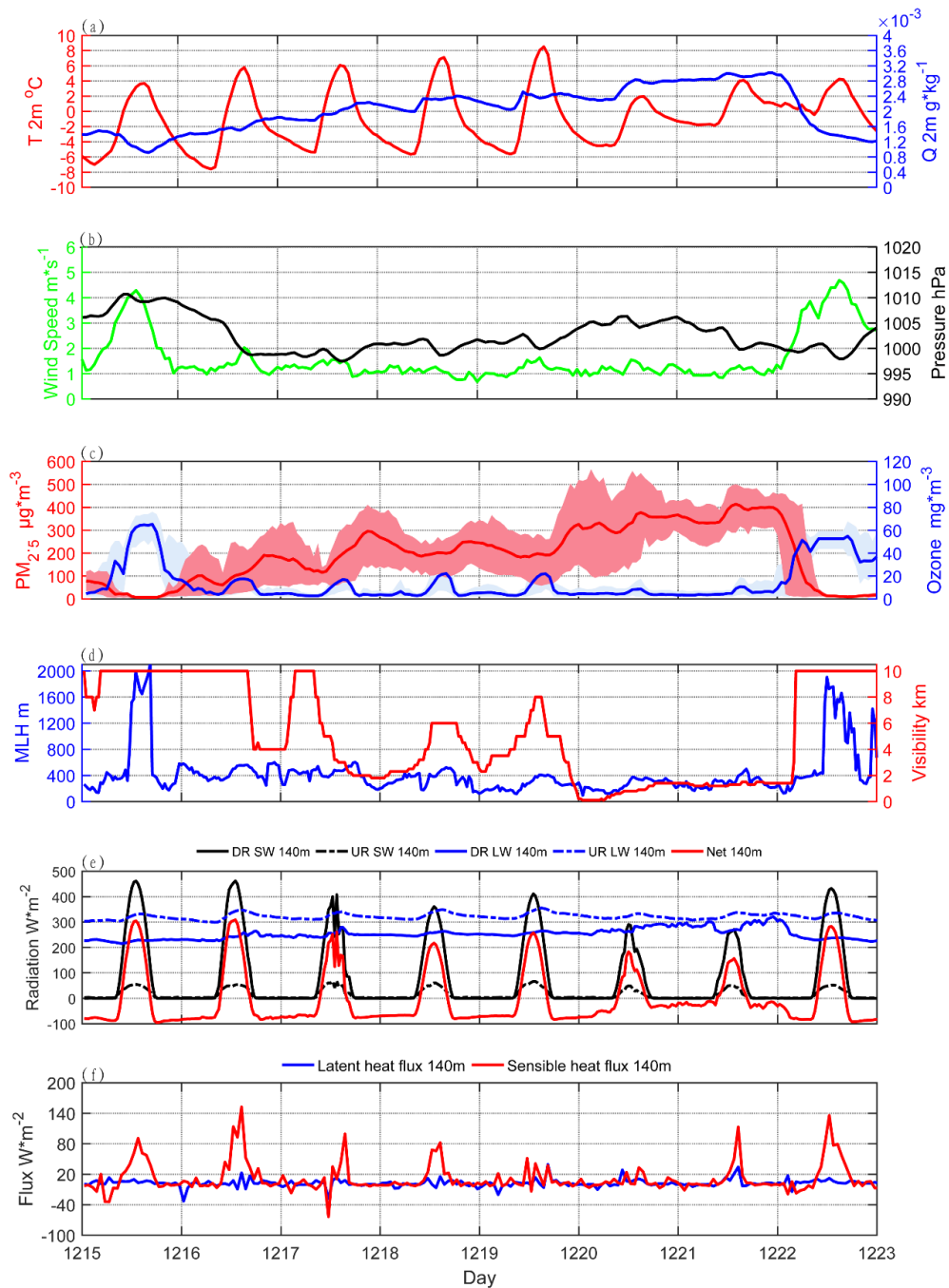


784

785 Figure 4 Hourly wind profile from the 15<sup>th</sup> to 23<sup>rd</sup> of December. Wind speed (shading;  $\text{m}\cdot\text{s}^{-1}$ ) and

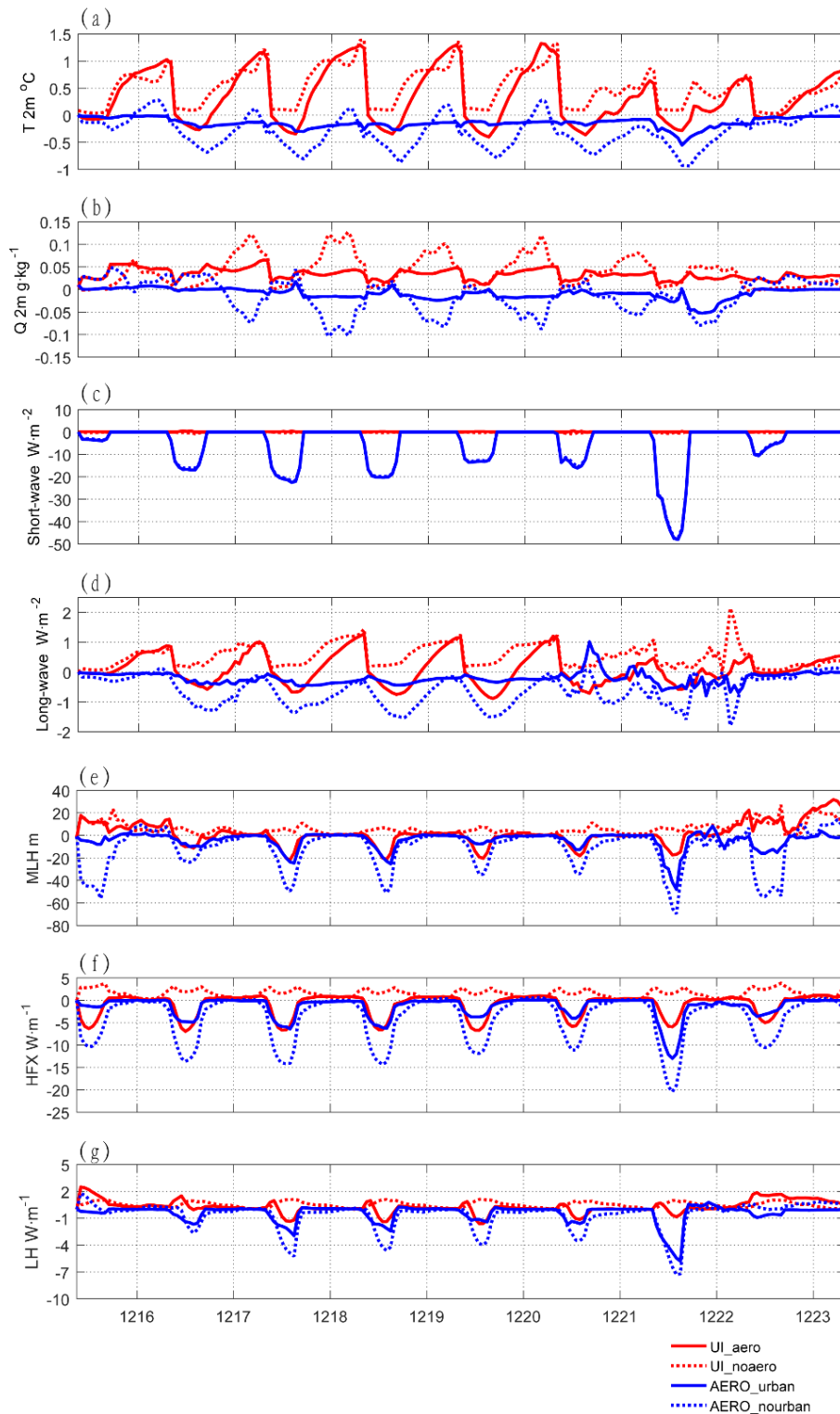
786 horizontal wind field (vector;  $\text{m}\cdot\text{s}^{-1}$ ). The black boxes show the two periods of south wind

787 conveyance.



788

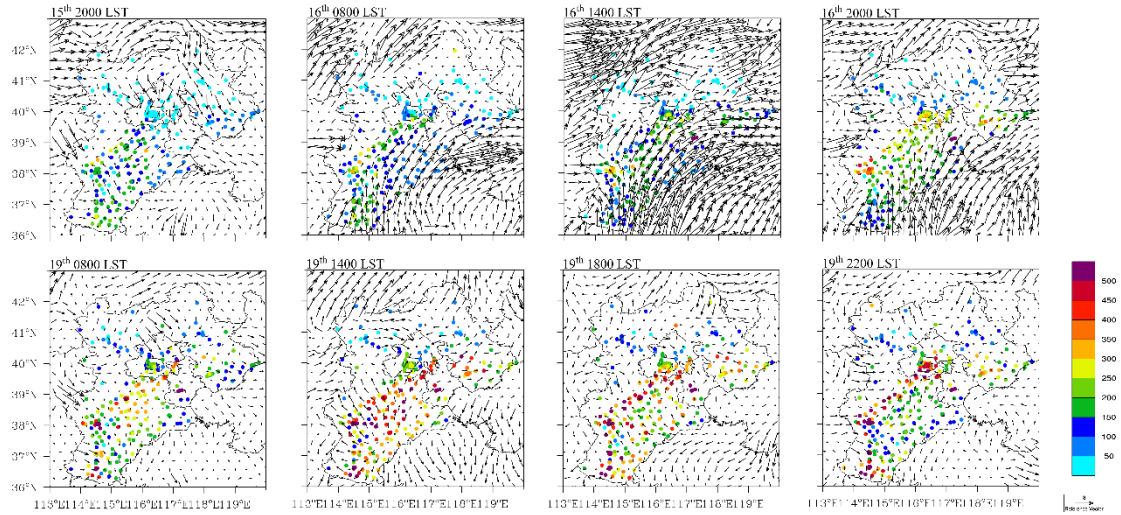
789 Figure 5 Diurnal pattern of observed variables from the 15<sup>th</sup> to 23<sup>rd</sup> of December in Beijing. (a)  
 790 Temperature (red line; °C) and absolute humidity (blue line; g kg<sup>-1</sup>) at 2 m; (b) wind speed at 10  
 791 m (green line; m s<sup>-1</sup>) and pressure (black line; hPa); (c) average PM<sub>2.5</sub> concentration (red line is  
 792 the average and the shading indicates the standard deviation; ug m<sup>-3</sup>) and ozone concentration  
 793 (blue lines and the shading indicate the standard deviation; mg m<sup>-3</sup>) of 35 environmental  
 794 monitoring stations in Beijing; (d) mixing layer height (blue line; m) and visibility (red line; km);  
 795 (e) radiation from the observation tower at 140 m, downward shortwave radiation (solid black  
 796 line; W m<sup>-2</sup>), upward shortwave radiation (dashed black line; W m<sup>-2</sup>), downward longwave  
 797 radiation (solid blue line; W m<sup>-2</sup>), upward longwave radiation (dashed blue line; W m<sup>-2</sup>), net  
 798 radiation (red line; W m<sup>-2</sup>); and (f) sensible heat flux (red line; W m<sup>-2</sup>) and latent heat flux (red  
 799 line; W m<sup>-2</sup>).



800  
801  
802  
803  
804  
805  
806

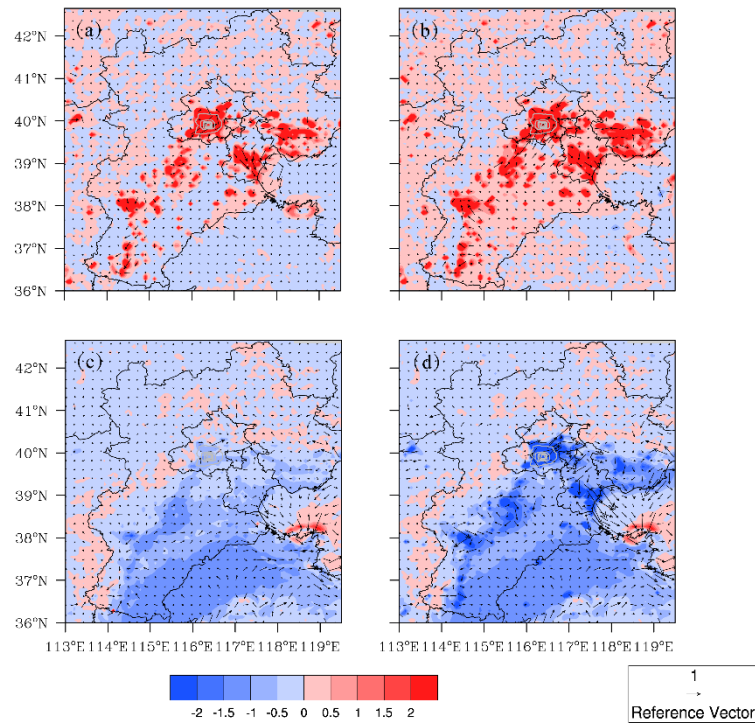
Figure 6 Diurnal patterns of simulated variables from the 15<sup>th</sup> to 23<sup>rd</sup> of December. (a) Temperature at 2 m (°C); (b) specific humidity ( $\text{g kg}^{-1}$ ) at 2 m; (c) shortwave radiation ( $\text{W m}^{-2}$ ); (d) longwave radiation ( $\text{W m}^{-2}$ ); (e) MLH (m); (f) sensible heat flux ( $\text{W m}^{-2}$ ); and (g) latent heat flux ( $\text{W m}^{-2}$ ).





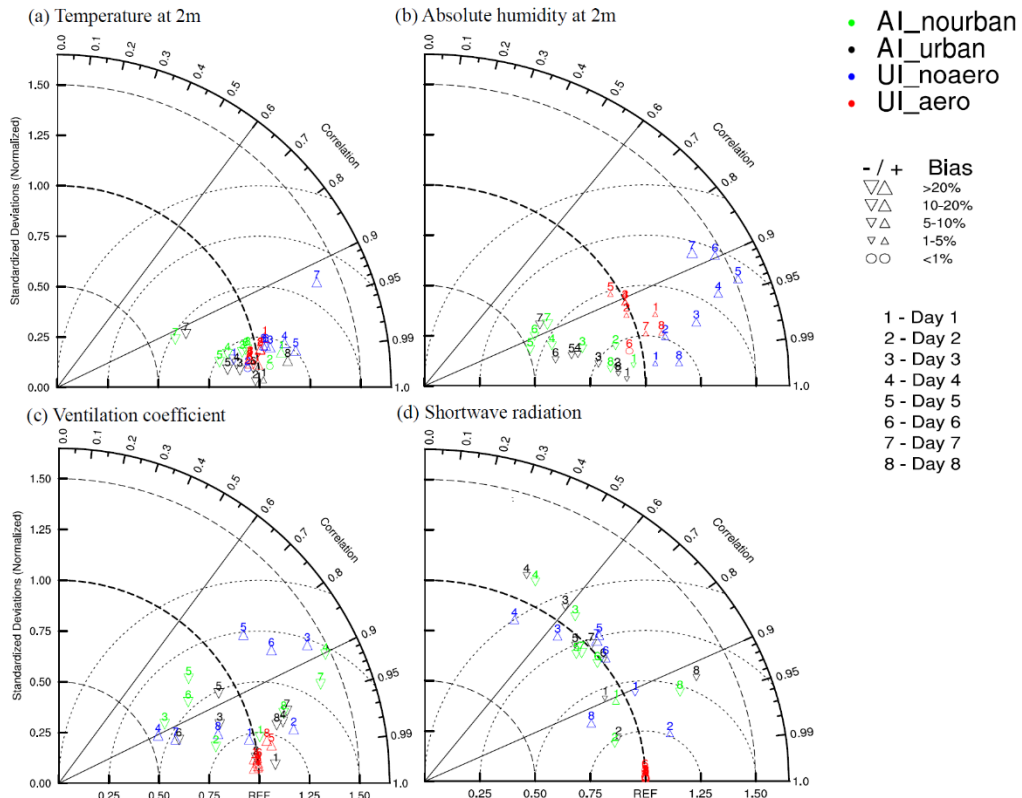
807  
808  
809  
810

Figure 7 Spatial distribution of the observed concentration of  $PM_{2.5}$  (dots;  $\mu g\ m^{-3}$ ) and wind field (vector;  $m\ s^{-1}$ ) for two increasing processes of the concentration of  $PM_{2.5}$ .



811  
812  
813  
814  
815  
816

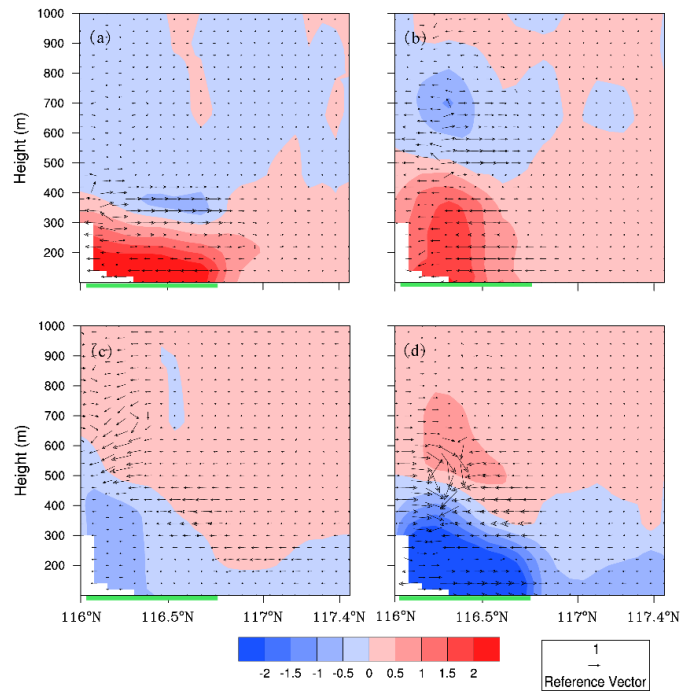
Figure 8 Spatial distribution of simulated temperature (shading;  $^{\circ}C$ ) and wind field (vector;  $m\ s^{-1}$ ). (a) UI\_aero; (b) UI\_noaero; (c) AI\_urban; (d) AI\_nourban.



817  
 818  
 819  
 820  
 821  
 822

Figure 9 Daily means of the four types of impacts (UI\_aero, UI\_noaero, AI\_urban, AI\_nourban) in the eight days are shown in Taylor diagrams in the Beijing area. (a) Temperature at 2 m ( $^{\circ}\text{C}$ ); (b) absolute humidity ( $\text{g kg}^{-1}$ ); (c) ventilation coefficient ( $\text{m}^2 \text{s}^{-1}$ ); (d) shortwave radiation ( $\text{W m}^{-2}$ ).





823

824

825 Figure 10 Cross section at 39.9°N of average temperature (shading; °C) and wind field (vector; m s<sup>-1</sup>) from 0000 LST to 0800 LST on the 16<sup>th</sup> to 20<sup>th</sup>. (a) UI\_aero; (b) UI\_noaero; (c) AI\_urban; (d)  
 826 AI\_nourban.  
 827

828

829

830

831

832

833

834

835